Increased sensitivity to myopia and altered retinal ON/OFF balance in a mouse model lacking *Dusp4*

Baptiste Wilmet[1*], Christelle Michiels[1], Jingyi Zhang[1], Awen Louboutin[1] Sanja Boranijasevic[1], Helen Frederiksen[1], Jacques Callebert[2], Juliette Varin[1], Marie-Laure Gimenez[1], Catherine Morgans[3], Robert Duvoisin[3], Linda Horan[4], Robin Plevin[4], Serge Picaud[1], Olivier Marre[1], Isabelle Audo[1,5], Christina Zeitz[1*].

*these authors contributed equally to this work and are corresponding authors

Author affiliations:

[1]Sorbonne Université, INSERM, CNRS, Institut de la Vision, Paris, France; [2]Service of Biochemistry and Molecular Biology, INSERM U942, Hospital Lariboisière, APHP, Paris, France; [3]Chemical Physiology and Pharmacology, Oregon Health and Science University, Portland, Oregon, USA; [4]Strathclyde Institute for Pharmacy and Biomedical Sciences, University of Strathclyde, Glasgow, Scotland; [5]CHNO des Quinze-Vingts, Centre de Référence Maladies Rares REFERET and INSERM-DGOS CIC 1423, Paris, France.

Email: christina.zeitz@inserm.fr, baptiste.wilmet@inserm.fr

Author Contributions: B.W., S.P., I.A. and C.Z. designed research; B.W., C.M., J.Z., S.B., A.L., H.F., J.C., J.V., F.B., M.-L.G., C.M., R.D., L.H., R.P, X.G. and O.M. performed research and/or analyzed data; B.W. and C.Z. wrote the paper. B.W. and C.Z. contributed equally to this work.

Competing Interest Statement: The authors have no competing interest to declare.

Keywords: Retina, myopia, cCSNB, electroretinography, dopamine

This PDF file includes:

Abstract (150 words)

Main Text (3894 words)

Material and methods (3000 words)

Figures 1 to 6

Supplemental figures 1 and 2

Legend for figures 1 to 6

Legend for supplemental figure 1 and 2

References (70)

Abstract

Myopia, influenced by environmental and genetic factors, occurs when the emmetropization process fails to stop, causing excessive eyeball growth. Highly myopic animal models lacking a functional ON-pathway identified *Dusp4* as a potential gene implicated in myopia. Here, we use a mouse model lacking DUSP4 to gain a better understanding of its retinal role and the mechanisms implicated in myopia development. *Dusp4*$^{-/-}$ mice have a reduced basal level of retinal dopamine and a higher susceptibility to lens-induced myopia. *Dusp4* is expressed in ON-bipolar cells and a subset of OFF-bipolar cells in a light dependent manner. The absence of DUSP4 causes a hyperactivation of the MAPK/ERK pathway. *Dusp4*$^{-/-}$ mice show a reduced optomotor response, increased ON-bipolar cell responses, reduced oscillatory potentials together with altered OFF and ON-OFF RGC response to light flashes. These data provide new insights into retina-driven mechanisms of myopization, nuancing the impact of ON and OFF pathways upon emmetropization.

Main Text

Introduction

Myopia -also known as shortsightedness- is the most common ocular dysfunction worldwide with a growing prevalence, especially in Southeast Asia [1, 2]. It is characterized by an abnormal increase in the axial length of the eyeball during refractive development (i.e. emmetropization), leading to blurry distance vision but normal near vision. Previous studies revealed that both environmental factors, such as light and genetic factors can be involved in myopia initiation and progression [3]. High myopia (<-6.00D) can lead to significant ocular complications that may cause severe vision loss and even blindness over time. Those include retinal detachment, myopic macular degeneration, choroidal neovascularization, glaucoma or early onset cataract. [4]. Given the major role of the retinal ON-pathway in perceiving light increments and the importance of light perception for proper emmetropization, studying myopia in the context of ON-pathway defects may offer new insight into the development of myopia.

In this respect, one form of inherited retinal disorders (IRDs), complete congenital stationary night blindness (cCSNB), caught our attention since it is associated with impairment of dim light vision and high myopia [5-7]. It is characterized by a complete loss of the b-wave upon electroretinography (ERG), in relation with ON-bipolar cell (ON-BC) pathway dysfunction [5]. ON-Cone Bipolar Cells (ON-CBCs) form direct excitatory synapses with dopaminergic amacrine cells (DACs). The retinal dopaminergic system, which is light dependent plays a critical role in proper emmetropization [8, 9]. Indeed, retinal levels of dopamine (DA), its metabolite 3,4-Dihydroxyphenylacetic acid (DOPAC) are considered as hallmarks of myopia. The precise mechanisms through which dopaminergic system impact emmetropization remains under debate but most likely involve dopamine receptors, especially D2R, expressed in several cell types such as RPE cells and photoreceptors[9, 10]. The main endpoint of the signaling cascade implies remodeling of the scleral extracellular matrix,

allowing the abnormal growth of the eyeball [11]. Both DA and DOPAC are reduced in a wide variety of experimental models of myopia [8, 9, 12, 13]. This also holds true for cCSNB mouse models, which show reduced levels of DA and DOPAC and are also more susceptible to develop myopia without necessarily displaying any detectable change in spontaneous refractive development [14-18]. The conjunction of pathways causing cCSNB and cCSNB-related myopia in both patients [5, 17] and animal models [14-18] raise the hypothesis that the different forms of cCSNB can lead to myopia through similar mechanisms and imply that ON-bipolar cell signaling influences the emmetropization process. It can be speculated that in these genetic models, the knockout of specific genes triggers a cascade of altered gene expression in the retina which contributes to the development of myopia. Similarly, the absence of light may induce comparable changes.

Our previous study performing whole RNA sequencing (RNAseq) on adult retinas from three cCSNB mouse models, *Gpr179*$^{-/-}$, *Lrit3*$^{-/-}$ and *Grm6*$^{-/-}$ and their corresponding wild type littermates (respectively *Gpr179*$^{+/+}$, *Lrit3*$^{+/+}$ and *Grm6*$^{+/+}$) revealed 52 differently expressed genes (DEGs) in at least two of those models [17]. Metanalyses showed that half of the DEGS were associated with the term “myopia” in the literature or human genome wide association studies [17]. Among those showing a lower expression compared to wild-type littermates, *Dusp4*, coding for the member of the dual specificity protein phosphatase subfamily 4 (DUSP4) (alias MKP-2), drew our attention based on the literature due to its unknown function in the retina and the availability of a knockout mouse model [19]. DUSP4 belongs to a group of DUSP phosphatases that inactivate their target kinases, e.g. mitogen-activated protein kinases (MAPKs), originally called extracellular signal-regulated kinases (ERKs). They are associated with cellular proliferation and differentiation by dephosphorylating both phosphoserine/threonine and phosphotyrosine residues. DUSP4 was shown to be expressed in different tissues and to have a role in innate and adaptive immunity [19], cancer [20], cardiovascular function [21], and brain [22]. Furthermore, its expression was found to be increased by multiple agents, including serum, growth factors, UV-light, and oxidative stress [23-25]. The role of DUSP4 in the retina has not been studied. However, our previous database search reveals that *DUSP4* is expressed in the retina and more specifically in rod ON-BCs (RBCs),

cone ON- and OFF-BCs, and in the retinal pigmented epithelium (RPE) [26]. It is noteworthy that induction of myopia by flickering light can be reduced by inhibiting phospho-ERK1/2 in guinea pigs [27]. In addition, retinal *Dusp4* expression appeared to be reduced upon induction of both Form Deprivation Myopia (FDM) and Lens Induced Myopia (LIM) in chicks and mice [28, 29]. Patients with a chromosomal 8p deletion, which includes the 8p12 *DUSP4*, often harbor eye defects including high myopia [30]. Here, we use mouse models lacking DUSP4 (*Dusp4*$^{-/-}$) or associated MAPK/ERK proteins (PKCα: *Pkcα*$^{-/-}$ and TPBG: *Tpbg*$^{-/-}$) and compared them to their wild type littermates (*Dusp4*$^{+/+}$, *Pkcα*$^{+/+}$ and *Tpbg*$^{+/+}$). We show that the most likely light dependent function of DUSP4 in the MAPK/ERK pathway is to support emmetropization and that the absence of DUSP4 activity increases susceptibility to myopia, possibly through an altered retinal ON/OFF balance.

Results

Disruption of the dopaminergic pathway in *Dusp4*$^{-/-}$, *Pkcα*$^{-/-}$ and *Tpbg*$^{-/-}$ mice.

As the dopaminergic pathway is altered in several models of myopia, we sought to measure retinal levels of DA and DOPAC in *Dusp4*$^{-/-}$, *Pkcα*$^{-/-}$ and *Tpbg*$^{-/-}$ mice. Ultra-Performance Liquid Chromatography (UPLC) measurements performed on isolated retinas from light-adapted adult *Dusp4*$^{+/+}$ and *Dusp4*$^{-/-}$ mice revealed a drastic reduction of both DA (Fig. 1A) and DOPAC (Fig. 1B) in *Dusp4*$^{-/-}$ compared to *Dusp4*$^{+/+}$ littermates (DA: 1267.3 ± 271.7 fmoles/retina in *Dusp4*$^{-/-}$, 2467.3 ± 186.1 fmoles/retina in *Dusp4*$^{+/+}$; DOPAC: 800.3 ± 70.1 fmoles/retinas in *Dusp4*$^{-/-}$, 253.0 ± 10.0 fmoles/retina in *Dusp4*$^{-/-}$). Similarly, retinal levels of DA and DOPAC were overall reduced in Pkc*α*$^{-/-}$ and *Tpbg*$^{-/-}$ mice, compared to their wild-type littermates (Supplemental Figure 1. DA: 1776,7 ± 45,9 fmoles/retina in *Pkcα*$^{-/-}$, 2770,6 ± 109,1 fmoles/retina in *Pkcα*$^{+/+}$, 2457;3 ± 50,8 fmoles/retina in *Tpbg*$^{-/-}$, 3111,3 ± 191,9 fmoles/retina in *Tpbg*$^{+/+}$. DOPAC: 444,4 ± 12,7 fmoles/retina in *Pkcα*$^{-/-}$, 715,3 ± 121,8 fmoles/retina in *Pkcα*$^{+/+}$, 656,0 ± 91,1 in *Tpbg*$^{-/-}$, 918,7 ± 71,9 fmoles/retina in *Tpbg*$^{+/+}$). These data suggest that the lack of DUSP4, PKCα or TPBG cause an alteration of the

dopaminergic pathway, which could impact the emmetropization process by impairing refractive development and increasing sensitivity to myopia induction.

Normal refractive development but increased sensitivity to LIM in *Dusp4*$^{-/-}$ mice.

To support *Dusp4* as a candidate gene for myopia, we measured refractive development and sensitivity to LIM of *Dusp4*$^{-/-}$ mice using an infrared photorefractometer. Measurement of the refractive state revealed that 3 weeks-old *Dusp4*$^{-/-}$ mice were slightly -but not significantly- more myopic than *Dusp4*$^{+/+}$ littermates (Fig. 1C). From 4 weeks to 9 weeks old, *Dusp4*$^{-/-}$ mice showed an overall normal refractive development with a hyperopic shift from 3 to 6 weeks followed by a plateau through 9 weeks of age (Fig. 1C). Following LIM induction, however, *Dusp4*$^{-/-}$ mice displayed a significantly greater myopic shift compared to *Dusp4*$^{+/+}$ littermates at 2 weeks which remained 3 weeks post goggling (Fig. 1D, -8.1±1.1 D in *Dusp4*$^{+/+}$, -11.7±1.1 D in *Dusp4*$^{-/-}$). These results suggest that the loss of DUSP4 in mice does not affect spontaneous refractive development but increases the sensitivity to LIM.

Expression profile and cellular immunolocalization of DUSP4 in the retina.

A recent RNAseq study of three cCSNB mouse models (*Gpr179*, *Lrit3* and *Grm6*) identified 52 differentially expressed genes, including *Dusp4* in at least two of the models, with a 1.2-fold change and a P-value of ≤ 0.01 [17]. *In situ* hybridization studies analyzed *Dusp4* mRNA at different developmental stages. At embryonic stage E15, *Dusp4* was expressed in the inner neuroblastic layer (INBL). At PN1 (PN= postnatal day), *Dusp4* was spread through both the outer neuroblastic layer (ONBL) and the INBL. From PN7 to PN66, *Dusp4* expression became more restricted to the outer part of the inner nuclear layer (INL) where BCs are located (Fig. 2A). Immunolocalization experiments confirmed BC localization of DUSP4 (Fig. 2B and 2C, green staining) in the INL, most likely in rod and cone ON-BCs. When retinal slices from *Dusp4*$^{+/+}$ and *Dusp4*$^{-/-}$ mice were co-immunostained against DUSP4 (green) and against PKCα, a marker of rod BCs, or against Goα, a marker for rod and cone ON-BCs (red), BC marker immunostaining surrounded the DUSP4

positive cells (Fig. 2B and 2C). All Goα and PKCα positive cells were DUSP4 positive cells, but we observed a small subset of DUSP4 positive cells that were not immunostained by anti-Goα or anti-PKCα located in the inner part of the INL, suggesting the presence of DUSP4 in a subset of amacrine cells (ACs) and/or OFF-BCs. DUSP4 immunostaining was absent in retinal slices of *Dusp4*$^{-/-}$ mice (Fig. 2B and 2C). Nonspecific immunostaining using the anti-DUSP4 antibody was observed in the outer plexiform layer in both *Dusp4*$^{+/+}$ and *Dusp4*$^{-/-}$ retinal slices. Western blot analysis of retinal extracts of *Dusp4*$^{+/+}$ revealed a band at 43 kDa, consistent with the predicted molecular weight of DUSP4. This band was absent in lanes from *Dusp4*$^{-/-}$ retinal samples (Fig. 2D), validating the absence of DUSP4 in *Dusp4*$^{-/-}$ mice. Quantification of DUSP4 protein levels through western blot in P14 and P40 wild-type retinas revealed no change of DUSP4 levels during development (Fig. 2E).

Impact of DUSP4 loss upon the retinal ERK/pERK pathway and the impact of light.

To examine whether the absence of DUSP4 alters the phosphorylation of MAPK/ERK, we performed western blot analyses with antibodies directed against ERK and its phosphorylated form: pERK (Fig. 2F). Relative to *Dusp4*$^{+/+}$ retinas, the pERK/ERK ratio was 2.98±0.37 in *Dusp4*$^{-/-}$ retinas, suggesting an overactivation of the ERK pathway. These findings confirm the important role of DUSP4 in inhibiting ERK phosphorylation in the retina.

As myopia development and progression is influenced by the light environment, and as *DUSP4* expression is induced by multiple agents including UV-light in other tissues, we investigated whether the quantity of DUSP4 is influenced by light. Although DUSP4 is detectable under dark conditions, DUSP4 levels were increased at 50 lux light-adapted retinas compared to dark-adapted retinas (Fig. 2G), suggesting that light can increase DUSP4 expression.

Cellular localization of DUSP4 loss in cCSNB mouse models.

As previously shown, *Dusp4* transcripts were reduced in cCSNB mouse models, *Gpr179*$^{-/-}$ and *Lrit3*$^{-/-}$ [17]. Here, we confirmed the reduction of *DUSP4* mRNA and protein levels (Fig. 3A and 3B)

in cCSNB retinas. To determine the cellular population directly affected by this reduction in DUSP4 in cCSNB mouse models, we performed co-immunostaining against DUSP4 with either Secretagogin (SCGNB), an EF-Hand Calcium Binding Protein and a marker of cone ON and OFF BCs, or ISLET1, a marker of all ON-BCs, ACs and retinal ganglion cells (RGCs) in adult *Lrit3*$^{+/+}$, *Lrit3*$^{-/-}$, *Gpr179*$^{+/+}$ and *Gpr179*$^{-/--}$ retinal slices (Fig. 3C to 3F). We observed a loss of DUSP4 immunostaining in both rod-BCs and cone ON-BCs in *Lrit3*$^{-/-}$ and *Gpr179*$^{-/-}$ retinas, whereas labeling of inner INL cells, most likely OFF-BCs or ACs, was little changed.

Impact of DUSP4 loss on mouse visual acuity.

To investigate whether the loss of DUSP4 leads to altered visual acuity, optomotor tests were performed with increasing spatial frequencies upon 6 week- and 6-month-old *Dusp4*$^{+/+}$ and *Dusp4*$^{-/-}$ mice under both photopic and scotopic conditions. Under both scotopic and photopic conditions, optomotor responses were unchanged in 6 weeks-old (Figs. 4A and B), but reduced in 6-month-old *Dusp4*$^{-/-}$ mice (Figs. 4C and D) compared to *Dusp4*$^{+/+}$ age-matched littermates at the lowest frequencies. The effect at 6 months was greater for scotopic than photopic responses. We did not observe any change in the spatial threshold (i.e. the lowest spatial frequency at which the mouse does not respond anymore), suggesting normal visual acuity. Altogether, these data suggest that the homozygous deletion of *Dusp4* causes an impairment of the optomotor response, more marked under scotopic conditions, and possibly in an age-dependent manner.

Retinal architecture in mice lacking DUSP4.

As functional disturbances can be correlated with morphological alterations, optical coherence tomography and eye fundus examinations were used to determine whether structural alterations could be observed in *Dusp4*$^{-/-}$ retinas (see Supplemental Figure 2 for an example with measurements of INL and IPL thickness). No obvious morphological alterations were observed in *Dusp4*$^{-/-}$ retinas at either 6 weeks or 6 months of age, suggesting that *usp4* ablation does not cause gross morphological changes.

Alteration of retinal signaling in mice lacking DUSP4.

In order to determine whether the genetic ablation of *Dusp4* could cause detectable alterations of retinal signaling, we performed full-field electroretinogram recordings on 6 week- and 6-month-old *Dusp4*$^{+/+}$ and *Dusp4*$^{-/-}$ mice (Fig. 5) and multiple electrode array (MEA) analyses on isolated retinas from 6-month-old *Dusp4*$^{+/+}$ and *Dusp4*$^{-/-}$ mice (Fig. 6). In 6-week-old *Dusp4*$^{+/+}$ and *Dusp4*$^{-/-}$ mice, no difference was observed in any of the ERG parameters tested (Fig. 5A to 5F). Fig. 5A and 5B show representative traces obtained at -1.5 log cd.s/m² (rod responses) and at 1.5 log cd.s/m² (mixed rod-cone responses). Unexpectedly, at 6 months of age, the amplitude of the b-wave was significantly increased in *Dusp4*$^{-/-}$ mice compared to *Dusp4*$^{+/+}$, without any statistically significant change in the a-wave. The implicit time of the b-wave was unchanged (Fig. 5G and 5H).

Furthermore, the amplitudes of the scotopic oscillatory potentials (OPs) of *Dusp4*$^{-/-}$ mice were significantly decreased at 6 months (Fig. 5O) without any change in their implicit time (Fig. 5N and 5M). The change in OPs suggests that *Dusp4* loss alters retinal signaling mediated by ACs, causing an improper response to light stimuli under scotopic conditions.

Full-field MEA recordings performed on dark-adapted 6-month-old *Dusp4*$^{-/-}$ retinas perfused with a normal recording medium (AMES) unveiled an unchanged spiking rate of ON-RGCs in response to light onset (Fig. 6A) but a markedly reduced spike rate of OFF-RGCs in response to light offset (Fig. 6C). Notably, a low number of *Dusp4*$^{-/-}$ OFF-RGCs were responsive (Fig. 6C, 6G and 6I). An increased ON-response, but reduced OFF-response of *Dusp4*$^{-/-}$ ON/OFF-RGCs was observed in response to light onset and offset, respectively (Fig. 6E), compared to *Dusp4*$^{+/+}$ mice. In addition, both ON- and OFF-responses of *Dusp4*$^{-/-}$ ON/OFF-RGCs showed a delayed return to baseline activity after onset of the corresponding stimulus (Fig. 6E). Under pharmacological blockade of the ON-pathway through L-AP4 perfusion, almost no ON- activity was recorded from both genotypes (Fig. 6B), as expected. A reduced spiking rate of *Dusp4*$^{-/-}$ OFF-RGCs was still observed, but a

higher number of *Dusp4*$^{-/-}$ OFF-RGCs were responsive to the stimulus (Fig. 6D, 6H and 6J). The spiking rate of the OFF-response of *Dusp4*$^{-/-}$ ON/OFF-RGCs was increased in the presence of L-AP4 (Fig. 6F) and a higher number of ON/OFF-RGCs were responsive, compared to wild-type (Fig. 6H and 6J). These data suggest that the loss of *Dusp4* induces an imbalance between ON- and OFF- pathway activity at the level of RGCs, which is most noticeable in OFF- and ON/OFF-RGCs.

Discussion

Despite a growing global awareness and improved medical care, the prevalence of myopia is increasing worldwide. Thus, further studies are required to gain a better understanding of myopia development and progression.

The reduced levels of retinal DA and the higher sensitivity of *Dusp4*$^{-/-}$ mice to LIM validated *Dusp4* as a myopia-associated gene. As in the present study, retinal DA metabolism is reduced in a wide variety of animal models of myopia [16, 18, 31-33]. In cCSNB patients and animal models, the loss of ON-pathway activity results in ablation of OPs [5, 34, 35], most probably due to a lack of excitatory input from ON-BCs to ACs. Lack of ON-BC-mediated activation of ACs including DACs, is the main hypothesis explaining the lack of DA release and thus, higher sensitivity to myopia in cCSNB mouse models [14-16, 18]. Strikingly, *Dusp4*$^{-/-}$ mice, even though they harbor a higher sensitivity to LIM, lower DA levels and reduced OP amplitude, also show a higher scotopic b-wave amplitude. This suggests an alternative chain of events is leading to myopia in *Dusp4*$^{-/-}$ eyes and excludes the candidacy of *Dusp4* as a cCSNB gene.

Consistent with previous findings [36], the amplitude of the ERG is age-dependent, irrespective of the presence of DUSP4. Nevertheless, its deletion leads to increased scotopic b-wave amplitude associated with reduced OPs at the highest stimulus intensities, strongly suggesting that the absence of DUSP4 causes an increased depolarization of ON-BCs in response to light. However, at these light intensities, both ON and OFF pathways contribute to the b-wave amplitude, in a positive and negative manner, respectively. Thus, as *Dusp4* is expressed in some subtypes of

OFF-BCs, we cannot exclude the implication of the OFF pathway in the increased b-wave through a lack of hyperpolarization possibly causing a delayed return to the baseline.

The impact of the MAPK/ERK pathway on retinal bipolar cells is unknown, but an increased pERK/ERK ratio such as reported in *Dusp4*$^{-/-}$ retinas, is thought to be associated with higher neuronal response [37]. Due to the excitatory nature of the ON-BC to DAC synapse, it is expected that a higher b-wave will increase rather than decrease DA release. Interestingly other animal models depleted for MAPK/ERK genes downregulated in cCSNB models, *Pkcα*$^{-/-}$ and *Tpbg*$^{-/-}$ mice revealed similar ERG phenotypes, lower retinal DA (Supplemental Figure 1) and are suspected to have a higher sensitivity to myopia induction [38-40]. We assume that a higher b-wave does not necessarily imply a higher glutamate release at the ON-BC to DAC synapse. TPBG, for instance, is implicated in neurotransmitter vesicle exocytosis and its loss can cause a reduced glutamate release from ON-BCs in *Tpbg*$^{-/-}$ mice despite a higher scotopic b-wave amplitude [39]. We hypothesize that similar mechanisms occur in those 3 models. Since *Dusp4*, *Prkca* and *Tpbg* have been linked to activation/deactivation of MAPK/ERK, they may overlap signaling pathways involving phosphorylation of presynaptic substrates by MAPK/ERK which has been shown to regulate synaptic transmission [41-43]. Furthermore, several studies unveiled a rapid increase of ERK phosphorylation following neuronal activation in mouse, rats and zebrafish models [44-46]. How this pathway influences refractive development and protection against myopia remains to be solved, but most likely involves the correct balance of MAPK/ERK activation/inactivation.

DUSP4 expression in other biological tissues is regulated by several factors including growth serum, oxidative stress, and UV light [21, 24, 47]. Our experiments add to these findings as retinal DUSP4 expression appears to be regulated by light. In addition, mice lacking ON-pathway activity show reduced DUSP4 expression in ON-BCs, with unchanged DUSP4 immunostaining in ACs or OFF-BCs (Fig. 3). Taken together, these findings suggest that 1) circadian rhythm, with changes in ambient light, may impact DUSP4 expression and 2) increased *Dusp4* expression in light-adapted retinas requires a functional ON-pathway. A recent study reported reduced *Dusp4*

expression in retinas from chick occluded eyes [48] in keeping with statement 1). Furthermore, it is conceivable that the remaining DUSP4 staining in dark adapted eyes is limited to OFF-BCs. Pronounced *Dusp4* mRNA staining in the INBL during embryonic stages and in INL at post-natal stages is consistent with previous analyses showing *Dusp4* expression in BCs in the adult retina [17, 49] as the INBL gives rise to RGCs, ACs and BCs [50]. According to databases [49] and our Immunolocalization study with specific markers, DUSP4 is not restricted to ON-BCs (RBCs and BC6 ON-CBC subtype) but is also expressed in some OFF-BCs (potentially BC2 and BC1B subtypes). This complexifies the putative role of *Dusp4* in the retina and pinpoints the need for investigations dissecting the specific role of DUSP4 in these cell types. For instance, previous studies have suggested that, in the mouse retina, BC2 OFF-BCs activity can affect ON-OFF direction sensitive ganglion cells (DSGCs) [51-53].

Our phenotyping experiments unveiled that *Dusp4*$^{-/-}$ mice have an overall lower optomotor response without any change in visual acuity. Our experimental paradigm implies a rotating velocity of about 12°/sec. At this velocity, ON-OFF DSGCs are known to be the major actors responsible for optomotor behavior [54-56]. Implication of *Dusp4* in ON-OFF DSGCs is supported by its expression in BC2 and BC1B CBCs as they contact ON-OFF DSGCs and the altered ON-OFF RGCs response observed in our MEA experiments. To our knowledge, altered ON-OFF DSGCs are not known to have any mechanistical relationship with myopia onset, thus, it is possible that our optomotor data highlight a new role for DUSP4 in retinal direction-selective circuit, independent from myopia itself.

The altered OFF and ON/OFF activity observed in our *Ex vivo* recordings from *Dusp4*$^{-/-}$ RGCs is consistent with the known expression of *Dusp4* in both ON- and OFF-BCs [49]. It is widely accepted that activation of the ON-pathway is independent of OFF-pathway activity, while activation of the OFF-pathway implies both an intrinsic activation of OFF-cells and a reduction of inhibition from the ON-pathway, mediated by inhibitory ACs [57, 58]. Thus, it is possible that the absence of DUSP4 in ON-BCs could give rise to changes in both ON- and OFF- spiking as observed in *Dusp4*$^{-/-}$ RGCs. Supporting this hypothesis, inhibiting the ON-pathway through L-AP4 perfusion

significantly increased the number of recordable OFF-RGCs in the *Dusp4*$^{-/-}$ retina. Overall, we hypothesize that the depletion of *Dusp4* causes an increased pERK/ERK ratio in both ON and OFF-BCs. This can increase the neuronal response of both ON and OFF-BCs but, as OFF-BCs activity is negatively impacted by ON-BC, and as ON-BCs are more numerous (≈70% of all BCs [59]), the potentially increased activity of OFF-BCs mediated by the higher pERK/ERK ratio might be countered by the inhibitory effect of the increased ON-BC activity. This is supported by the reduced *Dusp4*$^{-/-}$ OFF response observed in our MEA recordings and its recovery under L-AP4 perfusion. In addition, the partial recovery of the number of recordable *Dusp4*$^{-/-}$ OFF-RGCs under L-AP4 suggests that the reduced *Dusp4*$^{-/-}$ OFF activity is unlikely due to a loss of OFF-RGCs population.

To our knowledge, all mouse models with a selective ON-pathway defect show altered DA metabolism and higher sensitivity to myopia induction [14-18]. The impact of selective OFF-pathway defects is more controversial. For instance, mice lacking VSX1 with a mostly OFF-defect phenotype showed reduced retinal DOPAC levels but a normal sensitivity to form-deprivation myopia [60]. In contrast, overstimulation of the OFF-pathway induces a thinning of the choroid in humans and chickens [61] and some evidence suggests that myopia associated with a mutation in *GJD2* implies altered OFF-signaling [62]. The present results do not necessarily contradict these findings as we lack data about OFF-BC activity in *Dusp4*$^{-/-}$ mice. A mouse model lacking *Aplp2*, a myopia-associated gene, showed reduced b-wave from both rod pathway and mixed rod-cone pathway, decreased OPs, as well as a higher sensitivity to myopia induction, and a loss of OFF-CBC population [63, 64]. Overall, the data collected from *Aplp2*$^{-/-}$ mice [63, 64], patients with mutations in *GJD2* [62] and *Dusp4*$^{-/-}$ mice suggest that a complete loss of the ON-pathway is not the only retinal deficit causing myopia, as a higher ON-response and a lower OFF- response can also increase the sensitivity to myopia induction.

Altogether, this study and our previous work [17] confirm *Dusp4* as a gene implicated in the development of myopia and support the strategy of using myopia-associated IRD animal models to gain a better understanding of the mechanisms underlying syndromic and non-syndromic

myopia. Our findings highlight key factors such as light, retinal signaling, and genetics in the protection and development of myopia. Our work suggests potential therapeutic targets in retinal MAPK/ERK genes to control or prevent syndromic and non-syndromic myopia. In addition, here we report a more complex link between retinal network activity and myopia by involving the ON/OFF balance in the IPL, rather than sole ON pathway defect. Future studies should focus on other DEGs found in cCSNB [17] and on other IRDs associated with high myopia such as retinitis pigmentosa.

Materials and Methods

Animal Care and ethical statement

Animal procedures were performed according to the Council Directive 2010/63EU of the European Parliament, the Council of September 22, 2010, and on the ARRIVE guideline on the protection of animals used for scientific purposes. They were approved by the French Minister of National Education, Superior Education and Research. *Dusp4*$^{-/-}$ mouse model was generated previously [19]. Mouse lines and projects were registered as following: *Dusp4*$^{-/-}$: APAFIS#22074 *Gpr179*$^{-/-}$: APAFIS#18037, and *Lrit3*$^{-/-}$: APAFIS#18132, refractometry: APAFIS #27474.). Mice were kept in 12:12 hour light:dark cycles with mouse chow and water ad libitum.

Polymerase chain reaction (PCR) genotyping for *Dusp4*

DNA was extracted from mouse tails with 50 mM NaOH after incubation at 95°C for 30 min. Wild-type and mutant allele were amplified independently using a polymerase (HOT FIREPol, Solis Biodyne, Tartu, Estonia), two specific forward primers: m*Dusp4*_3F (5'-GTCTAGAAAGCCTTTCCGTC-3') for the wild-type allele and m*Dusp4*_F3 (5'-GATCCGATAACTTCGTATAGC-3') for the mutant allele and two specific reverse primers: m*Dusp4*_3R (5'-GCGCCTAACGCCTAAAATCC-3') for the wild-type allele and m*Dusp4*_4R (5'-GTAAAACAGGAGCTGGCATC-3') for the mutant allele. The following PCR program was used: 15 min at 95°C for denaturation, 35 cycles of: 45 sec at 95°C, 1 min at 58°C, and 1 min 30 sec at 72°C, and for final extension, 10 min at 72°C. This gives rise to the following amplicons: PCR using m*Dusp4*_3F and m*Dusp4*_3R primers amplifies a product of 386 base pairs (bp) for the wild-type allele and no product for the mutant allele, PCR using m*Dusp4*_F3 and m*Dusp4*_4R primers amplifies no product for the wild-type allele and a 1000 bp product for the mutant allele. PCR products were separated by electrophoresis on 2% agarose gels, stained with ethidium bromide, and visualized using a documentation system (Molecular Imager® Gel Doc™ XR+ System, Bio-Rad, Hercules, California, USA).

Induction and measurement of myopia in *Dusp4*$^{-/-}$ mice

Lens induced myopia

The lens induced myopia protocol was adapted from a previously validated protocol [65]. Briefly, P21 mice were anesthetized by isoflurane inhalation (5% induction, 2% maintenance). The scalp was cut to expose 1.2 cm of the skull in the rostrocaudal axis. Two intracranial screws were implanted on both left and right sides of the skull at y = -2 mm from the bregma. A homemade goggle frame was placed on the skull and fixed using dental cement (FujiCEM™, Phymep© Cat #900903, Paris, France). The goggle frame, adapted from [45], was built in resin using a 3D printer. -25 D lenses were stuck on the frame using glue (vetbond™, Phymep©, Paris, France). Stitches were used to avoid displacement of lens by mice. The -25 D lens was always placed in front of the right eye for three weeks.

Refractometry

After a dark adaptation period of 30 min, eye drops were used to dilate the pupils (0.5% mydriaticum, 5% neosynephrine). The mice were placed on a homemade restraining platform in front of an eccentric infrared photorefractometer; its calibration was described elsewhere [66]. The mouse was positioned so that the first Purkinje image was in the center of the pupil. The data were then recorded using software designed by Franck Schaeffel [66]. We collected two data sets per animal, one per eye, each data set consisting of 90 measures, each of which being the mean of 10 successful measures. For refractive development experiments, the measurements were performed once per week, every week from 3 to 9 weeks old and the mean between both eyes was used for statistical analysis. To evaluate the sensitivity to myopia induction, the difference between goggled and ungoggled eyes measured at P21 (day of surgical procedure), P35 (14 days after surgery) and P42 (21 days after surgery) was used for statistical analysis. Only the non-myopic mice displaying less than 2D of interocular shift at P21 were used for the induction protocol. Values are presented as mean± SEM. Statistical significance was tested using a Two-way ANOVA.

DA and DOPAC measurements

The light adaptation and the measurement of retinal levels of DA and DOPAC were performed as previously described [16]. Values are presented as mean± SEM. Statistical significance was evaluated using a Mann-whitney test.

Western blot quantification of DUSP4 protein and pERK/ERK ratio

Preparation of retinas for protein extraction for western blot analyses

Whole retina samples were lysed with lysis buffer (Tris 50 mM pH7.5, NaCl 150 mM, Triton X100 1%) for 30 min on ice, vortexed every 10 min. Samples were thereafter sonicated 3x10 sec, with 30 sec on ice between each sonication. Soluble proteins were recovered from the supernatant following a 10-min centrifugation (13,000 rpm) at 4°C. The concentration of protein in each sample was determined by a bicinchoninic acid (BCA) assay and samples were kept at -80°C until required.

Western blot analyses

Equal concentrations (6µg) of protein extracted from whole retina of wild-type and *Dusp4*$^{-/-}$ mice, were separated by electrophoresis on a commercially available 1 mm protein gel (NuPAGE™ 4-12% Bis-Tris Gel, Invitrogen, Waltham, MA, USA). The proteins were transferred to a 0.2 µm nitrocellulose membrane (Trans-Blot Turbo Mini Nitrocellulose membrane, Bio-Rad, Hercules, CA, USA) using a semi-dry transfer system (Trans-Blot® Turbo, Bio-Rad) and blocked in 5% dry milk (Regilait, Saint-Martin-Belle-Roche, France) in phosphate-buffered saline containing 0.05% Tween-20 (PBST) at room temperature (RT) for 1 hour. Membranes were incubated with the primary antibodies consecutively at 4°C overnight. Description of the primary antibodies, their dilution and references can be found in Supplemental table 1. Subsequently, the membranes were washed three times with PBST and incubated with the corresponding anti-rabbit, -mouse or -goat horseradish peroxidase (HRP) secondary antibodies (1/10,000) for 1 hour at RT. After three washes in PBST, membranes were incubated with enhanced chemiluminescence (ECL) substrate

for 5 min. Antibody binding was thereafter detected in a dark room using a commercially available developer (Kodak, Rochester, NY, USA).

Protein quantification:

Protein quantification was done using western blot images and by a commercial software (ImageJ, National Institutes of Health, Bethesda, MD, USA). Subsequently graphs were statistically analyzed using a statistics and graphing software (Prism 9.1.2, GraphPad). Data were tested for normality and analyzed using the nonparametric Mann-Whitney test to compare ranks. Values are reported as mean ± standard error means (SEM). Statistical significance was obtained with $P \leq 0.05$ for *, $P \leq 0.01$ for **, $P \leq 0.001$ for *** and $P \leq 0.0001$ for ****.

Antibody	**Size (kDa)**	**Dilution**	**Host**	**Reference**	**Manufacturer**
DUSP4	43	1/500	Rabbit	ab216576	Abcam
GAPDH	36	1/200	Goat	SC-20357	Santa Cruz
PKCα	80	1/500	Mouse	P5704	Sigma-Aldrich
G0α	40	1/200	Mouse	MAB3073	Merck Millipore
ISLET1	39	1/500	Mouse	Ab86501	Abcam
SCGN	32	1/100	Mouse	AMAb90630	Sigma Aldrich
PERK	42,44	1/1000	Rabbit	9101S	Cell Signaling
ERK	42,44	1/1000	Rabbit	4695T	Cell Signaling

Preparation of retinal sections for localization of *Dusp4* protein and RNA.

Preparation of retinal sections

Retinal slices of 6-week-old *Dusp4*$^{-/-}$, *Gpr179*$^{-/-}$ and *Lrit3*$^{-/-}$ mice and their corresponding wild-type controls were obtained according to a protocol adapted from [67]. Briefly, Mice were sacrificed by

CO2 inhalation followed by cervical dislocation. For hybridization in situ (ISH) entire eyes were isolated, a hole was performed just behind the ora serrata and then eye was fixed in 4% paraformaldehyde (PFA) at RT during 20 minutes. After fixation the eye was washed three times in PBS and put directly on 30% cold sucrose solution for the cryoprotection.

For immunoimmunolocalization studies the anterior segment and lens were removed, and the eyecup was fixed in cold 4% PFA for 20 minutes. After three washing with cold PBS, eyecups were cryoprotected with increasing concentrations of sucrose (10% and 20% for 1h each and 30% overnight).

To finish, the entire eye for ISH or the eyecups for immunolocalization were embedded in 7.5% gelatin 10% sucrose and frozen in a dry ice-cooled isopentane bath. Sections were cut at a thickness of 20 µm on a cryostat (model HM560, Microm; Thermo Fisher, Walldorf, Germany). and mounted onto glass slides (Super-Frost plus Gold for ISH and Super-Frost plus for immunolocalization, ThermoFisher Scientific,Waltham, MA, USA). The slides were air dried and stored at 80 °C

In situ hybridization procedure

RNA in situ hybridization was performed on adult mouse retinal section (20µM). The mouse cDNA corresponding to *DUSP4* exon 1-4 was cloned in a plasmid pBluescript II SK by Genecust company (Genecust, Boynes, France). The antisense and sense probes were obtained after plasmid was linearized using the restriction enzymes NotI and KpnI. Antisense and sense RNA in situ hybridization probes were synthesized using T7 and T3 RNA polymerase (Roche Diagnostics, Basel, Switzerland), respectively, and labeled with digoxigenin-UTP (Roche Diagnostics). Mouse retinal sections were postfixed 10 minutes in 4% PFA, washed with PBS, and treated with proteinase K (10mg/mL; Invitrogen, Carlsbad, Czech Republic) for 2 minutes. Following a wash with PBS, the sections were postfixed in 4% PFA, washed in PBS, and then acetylated in an acetylation buffer of 1.3% triethanolamine (Sigma-Aldrich, St. Quentin Fallavier, France), 0.25% acetic anhydride (Sigma-Aldrich), and 0.06% hydrochloric acid solution. The sections were washed

in 1% Triton X-100 PBS solution and blocked for 2 hours in hybridization buffer containing 50% formamide, 5X SSC (saline sodium citrate [1X SSC is 0.15 M NaCl plus 0.015 M sodium citrate]), 1X blocking solution (Denhardt's solution; Sigma-Aldrich), 250 µg/mL yeast tRNA (Roche Diagnostics), and 240 µg/mL salmon sperm (Roche Diagnostics), pH 7.4. The sections were hybridized with digoxigenin-labeled probes overnight at 72°C, after which they were rinsed for 2 hours in 0.2% SSC at 72°C and blocked for 1 hour at RT in 0.1 M Tris, 0.15 M NaCl (B1), 10% normal goat serum (NGS; Vectorshield, Burlingame, CA), pH 7.5. After blocking, slides were incubated overnight at RT with anti-digoxigenin antibody conjugated with alkaline phosphatase (1:5000 dilution; Roche Diagnostics) in B1 containing 1% NGS. After additional washes, the alkaline phosphatase activity was detected using nitro blue tetrazolium chloride (337.5 mg/ml; Roche Diagnostics) and 5-bromo-4-chloro-3-indolyl phosphate (175 lg/ml; Roche Diagnostics). Five hours later, sections were mounted in Mowiol (Calbiochem, Merck, Carlstadt, NJ). Slides were scanned with a Nanozoomer 2.0 high throughput (HT) equipped with a 3- charge–coupled device time delay integration (TDI) camera (Hamamatsu Photonics, Hamamatsu, Japan).

Immunohistochemistry procedure

Retinal slices of *Dusp4*$^{-/-}$, *Gpr179*$^{-/-}$ and *Lrit3*$^{-/-}$ mice and their corresponding wild-type littermates were placed in a humid chamber. Slices were saturated using a PBSGT solution (PBS1X, 0.2% gelatin, 0.25% TritonX100) overnight at RT. Incubation with primary antibodies diluted in PBSGT lasted overnight at RT. Description of primary antibodies can be found in supplemental table 1. After washing in PBS 0.1% TritonX100, the sections were incubated with corresponding secondary antibodies coupled to Alexa Fluor 488 or Alexa Fluor 594 (Jackson Immuno Research Laboratories, Baltimore, MD, USA) at a dilution of 1:1000 in PBSGT for 1h at RT. The slides were stained with 40,6-diamidino-2-phenylindole (DAPI) sections were washed 3 times in PBS and mounted with cover-slipped with mowiol (Calbiochem, Merck, Carlstadt, NJ). Images were acquired using a confocal microscopy (Olympus FV1200, Rungis, France).

Quantification of Dusp4 mRNA

Preparation of retinas for RNA extraction

RNA extraction of whole retina samples was performed according to manufacturer's instructions (RNeasy Protect Mini Kit, Qiagen, Hilden, Germany). The Dnase elimination step was included and followed according to the manufacturers' protocol. A final volume of 40 µl was eluted using Rnase-free water. The RNA yield was analyzed via spectrophotometric absorbance (Nanodrop™ 2000, Thermo Fisher Scientific, Waltham, MA, USA), with suitable concentration being above 200 ng/µl. Extracted RNA was kept at -80°C until required.

Real Time PCR (RT-PCR)

RT-PCR was performed on extracted RNA from whole mouse retinas. The quality of RNA in each sample was first tested on a bioanalyzer (Agilent 2100 Bioanalyzer, Agilent Technologies, Santa Clara, CA, USA) according to manufacturer's instructions (Agilent RNA 6000 Nano Kit, Agilent). Samples with a RIN <7 were discarded. A two-step RT-PCR was then performed using RNAs with concentrations of 50 ng/µl for each sample and 5 ng/µl for the negative controls. RNAs were reverse transcribed into single-stranded cDNA according to the kit protocol (QuantiTect® Reverse Transcription, Qiagen). The cDNA was first diluted to a concentration of 2 ng/µl for each sample and 0,5 ng/µl for the negative control samples. The PCR reaction solutions each contained 5µl cDNA, 10 µl SYBR Green, 0,4µl of each primer (Table 2) and 4,2 µl H2O, for a total reaction volume of 20 µl. Each RT-PCR reaction was performed in triplicates for both the wild type (wt) and the mutant mouse, with glyceraldehyde-3-phosphate dehydrogenase (GAPDH) used as a reference gene. The detailed protocol of the PCR-conditions will be delivered on request.

Gene	**Primer Name**	**Primer Sequence (5'-3')**
Gapdh	GAPDH_F	TGTGTCCGTCGTGGATCTGA
	GAPDH_R	TTGCTGTTGAAGTCGCAGGAG

Dusp4	DUSP4_EX3-4FA	CGAGTACATCGACGCAGTAAAG
	DUSP4_EX4RA2	CAGATGGTGGCTGATCGGG

Phenotyping of *Dusp4*$^{-/-}$ mice

Optomotor response

6-week-old or 6-month-old mice were dark-adapted overnight before the optomotor test. Mice were placed on a grid platform at the center of a motorized drum (adapted from [68]) revolving clockwise and anticlockwise at two revolutions per minute and covered by vertical black and white stripes of a defined spatial frequency (0.063, 0.125, 0.25, 0.5 and 0.75 cycles per degree (cpd)). Each test was recorded with a digital infrared camera to count head movements of the mice. Head movements in both directions were considered to obtain the number of events per minute. Values are presented as mean± SEM. Statistical significance was tested using a two-way ANOVA.

Electroretinography

After overnight dark adaptation, 6-week-old or 6-month-old mice were anesthetized with ketamine (80mg/kg, Axience, France) and xylazine (8mg/kg, Bayer HealthCare, France). Eye drops were used to dilate the pupils (0.5% mydriaticum, Thea, France and 5% neosynephrine, CSP, France) and anesthetize the cornea (0.4% oxybuprocaïne chlorhydrate, Thea, France). Upper and lower lids were retracted to keep eyes open and bulging. Contact lens electrodes for mice (Mayo Corporation, Japan) were placed on the corneal surface to record ERG responses through a layer of Lubrithal (Dechra Veterinary Products, Denmark). Needle electrodes placed subcutaneously in forehead and in the back served as reference and ground electrodes. Stimulus presentation and data acquisition were provided by the Espion E2 system (Diagnosys LLC, Lowell, MA, USA). For the dark adapted ERG recordings, a cut-off filter of 0.312-300Hz (low-high) was applied and eight levels of stimulus intensity ranging from 0.0006 cd.s/m^2 to 60 cd.s/m^2 were used. Each scotopic

ERG response represents the average of five responses from a set of five flashes of 4ms stimulation. Oscillatory potentials were recorded under dark condition. A cut-off filter of 75-300Hz (low-high) was applied to the signal and an average of five responses to a set of five flashes of 4ms stimulation at 60 cd.s/m^2 was obtained. Values are presented as mean± SEM. Statistical significance was tested using a Mann-Whitney test.

Spectral Domain-Optical Coherence Tomography (SD-OCT)

6-week- or 6-month-old mice were anesthetized by isoflurane inhalation (5% for induction, 2% to maintain). Eye drops were used to dilate the pupils (0.5% mydriaticum, 5% neosynephrine). SD-OCT images were recorded for both eyes using a spectral domain ophthalmic imaging system (Bioptigen, Inc., Durham, NC, USA). We performed rectangular scans consisting of a 1.4 mm by 1.4 mm perimeter with 1000 A-scans per B-scan with a total B-scan amount of 100. Scans were obtained first while centered on the optic nerve, and then with the nerve displaced either temporally/nasally or superiorly/inferiorly. We measured the thickness of Retinal Nerve Fiber Layer and Ganglion cell layer together (RNFL+GCL), Inner plexiform Layer (IPL), Inner Nuclear Layer (INL), Outer Plexiform Layer (OPL), Outer Nuclear Layer (ONL), External Limiting Membrane (EML), Inner Segment and Outer Segment together (IS+OS) and Retinal Pigment Epithelium and Choroid together (RPE+C). Values are presented as mean± SEM. Statistical significance was tested using a two-way ANOVA.

Assessment of *Dusp4*$^{-/-}$ retinal circuitry using Multi-electrode array (MEA).

Tissue preparation, and stimulation protocol were performed as previously described [69]. After overnight dark adaptation, mice were euthanized by CO_2 inhalation followed by cervical dislocation. Retinas were carefully dissected under dim-red light and conserved in Ames medium (Sigma-Aldrich, St. Louis, MO, USA) oxygenated with 95% oxygen and 5% CO_2. Retinas were placed on a Spectra/Por membrane (Spectrum Laboratories, Rancho Dominguez, CA, USA) previously coated with poly-D-lysine and pressed against an MEA (MEA256 100/30 iR-ITO; Multi Channel

Systems MCS, Reutlingen, Germany) using a micromanipulator, RGCs facing the electrodes. Retinas were continuously perfused with bubbled Ames medium or L-AP4 (50µM, Tocris, Bristol, UK) at 34.8°C at a rate of 2 ml/min and let to rest for 45 min before the recording session. Under dark conditions, 10 repeated full-field light stimuli at a 450 nm wavelength were applied to the samples at 4.85^13 photons/cm^2/s for 2 seconds with 10-seconds interval by using a Polychrome V monochromator (Olympus, Hamburg, Germany) driven by an STG2008 stimulus generator (MCS). Raw RGC activity recorded by MEA was amplified (gain 1000–1200) and sampled at 20 kHz using MCRack software (MCS).

The resulting data was high-pass filtered at 100 Hz, and spikes were detected using SpyKING CIRCUS [70]. Only cells presenting a low number of refractory period violations (inferior to 0.5%, 2ms refractory period) and well-distinguished template waveforms were selected for analysis, giving a total of 887 cells (526 from two *Dusp4*$^{+/+}$ mice and 361 from two *Dusp4*$^{-/-}$ mice). These criteria ensured the high quality of the reconstructed spike trains. Subsequent analysis was performed using custom Python scripts.

We determined for each sorted RGC the maximum firing frequency in an interval of 2 seconds after light onset (for ON-responses) and in an interval of 2 seconds after light offset (for OFF-responses). These values were normalized to the mean spontaneous firing frequency of the corresponding RGC. Considering that significant responses have a maximum firing frequency that is superior to the mean spontaneous firing frequency +5 SD, we determined the time at which these significant frequencies were reached after the light onset for ON-responses and after the light offset for OFF-responses. We computed an ON-OFF index $I_{ON\text{-}OFF}$ for each cell with the following formula: $I_{ON-OFF} = (n_{light} - n_{dark}) \div (n_{light} + n_{dark})$ with n_{light} the number of detected spikes during the light onset and n_{dark} those detected for the same duration after the light offset. Cells having a $I_{ON\text{-}OFF}$ close to -1 would be considered OFF cells, while those having a $I_{ON\text{-}OFF}$ close to 1 would be ON cells. Here we considered cells as OFF with $I_{ON\text{-}OFF}$<-0.5, ON with $I_{ON\text{-}OFF}$>0.5, and ON-OFF in between.

Funding

Supported by Agence Nationale de la Recherche (ANR-22-CHIN-0006) (OM, CZ); Banque publique d'investissement (PREMYOM), Retina France; Valentin Haüy and AFM (CZ), IRPINSERM (CZ and RD); Prix Dalloz pour la recherche en ophtalmologie and Fondation Dalloz—Institut de France (CZ); Fondation Voir et Entendre (CZ); Fondation de l'oeil—Fondation de France (IA, CZ), Ville de Paris and Region Ile de France; Labex Lifesenses (reference ANR-10-LABX-65), supported by French state funds managed by the ANR within the Investissements d'Avenir programme (ANR-11-IDEX-0004-0); the Programme Investissements d'Avenir IHU FOReSIGHT (ANR-18-IAHU-01); National Institutes of Health grant EY029985 (RD), funded by the European Union under Grant Agreement #101119501 (SB).

Figures and Tables

Figure 1: Myopic traits observed in *Dusp4*$^{-/-}$ mice.

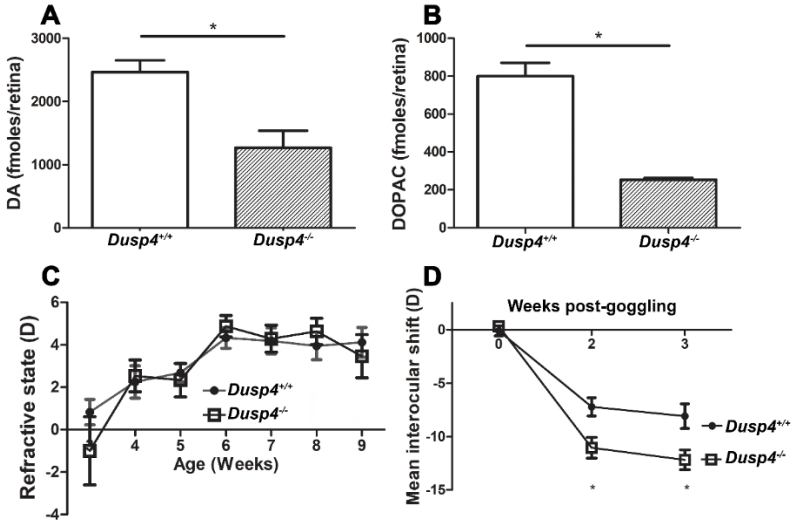

A and B: Measurement of retinal levels of DA (A, n=3) and DOPAC (B, n=3) in adult light-adapted *Dusp4*$^{+/+}$ (n=3) and *Dusp4*$^{-/-}$ (n=3) mice using UPLC. C: Measurement of spontaneous refractive development of *Dusp4*$^{+/+}$ (n=21) and *Dusp4*$^{-/-}$ (n=20) mice using infrared refractometry. D: Measurement of the mean interocular shift induced by LIM in *Dusp4*$^{+/+}$ (n=9) and *Dusp4*$^{-/-}$ (n=9) mice. *: P≤ 0.05.

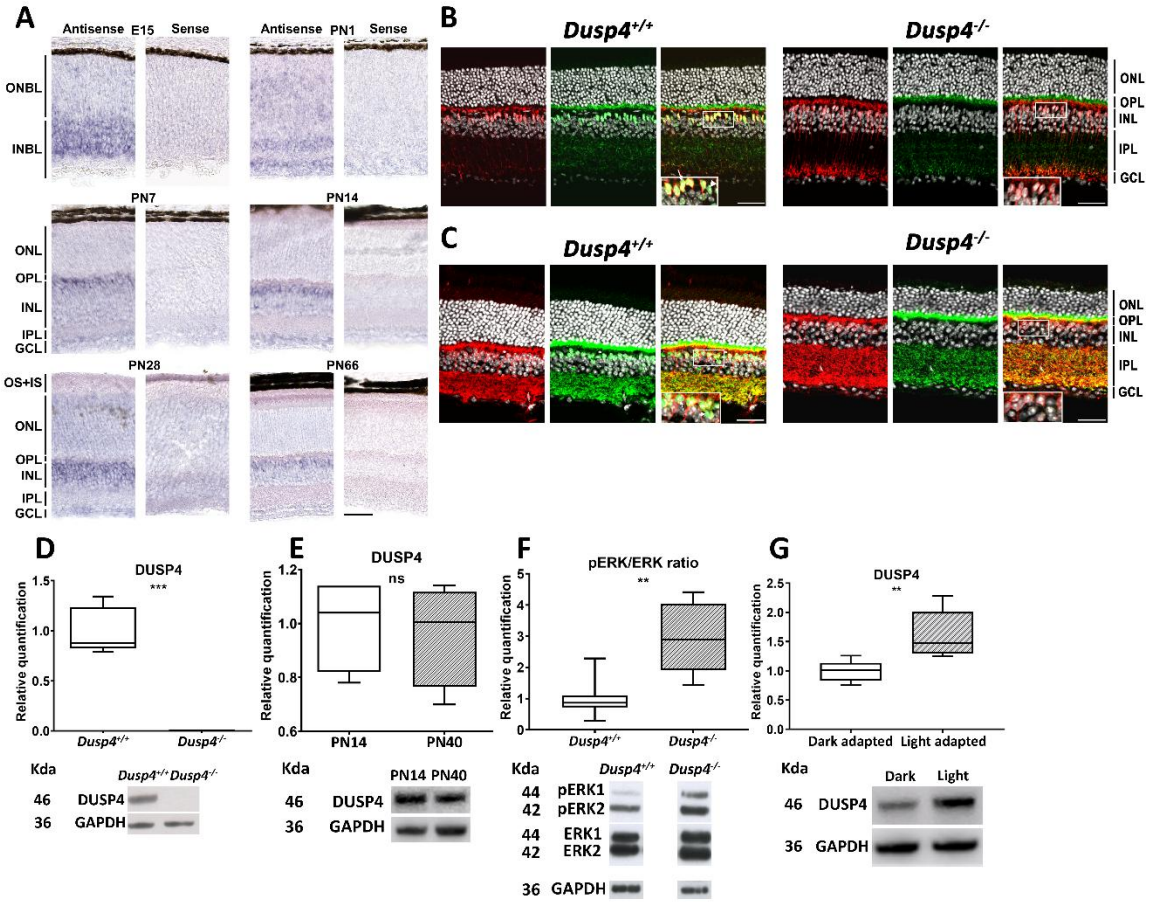

Figure 2: Retinal expression of DUSP4.

A: ISH targeting *Dusp4* mRNA performed on wild-type retinal slices at various developmental stages (E15, PN1, PN7, PN14, PN28 and PN66). B: co-immunostaining of DUSP4 (green) with PKCα (red) performed on adult retinal slices from either *Dusp4*$^{+/+}$ (left) or *Dusp4*$^{-/-}$ (right) mice. C: co-immunostaining of DUSP4 (green) with G0α (red) performed on adult retinal slices from either *Dusp4*$^{+/+}$ (left) or *Dusp4*$^{-/-}$ (right) mice. D: Relative quantification of DUSP4 through western blot analysis performed on isolated adult retinas from either *Dusp4*$^{+/+}$ (n=5) or *Dusp4*$^{-/-}$ (n=5) mice. E: Relative quantification of DUSP4 protein through western blot analysis performed on isolated retinas from either PN14 (n=4) or PN40 (n=4) mice. F: Relative quantification of pERK/ERK ratio through western blot performed on isolated adult retinas from either *Dusp4*$^{+/+}$ (n=7) or *Dusp4*$^{-/-}$ (n=9) mice. G: Relative quantification of DUSP4 protein through western blot analysis performed on adult wild-type isolated retinas under either dark adaptation (n=6) or 50 lux light adaptation

(n=7). ONBL= Outer Neuroblastic Layer, INBL= Inner Neuroblastic Layer, ONL= Outer Nuclear Layer, OPL= Outer Plexiform Layer, INL= Inner Nuclear Layer, IPL= Inner Plexiform Layer, GCL= Ganglion Cell Layer. Scale bars= 50µm. Arrowheads= Potential OFF BCs (DUSP4 positive, PKCα or G0α negative), arrows= ON-BCs (DUSP4 positive, PKCα or G0α positive). D-G: ns: non-significant, **: P≤ 0.01, ***: P≤ 0.001.

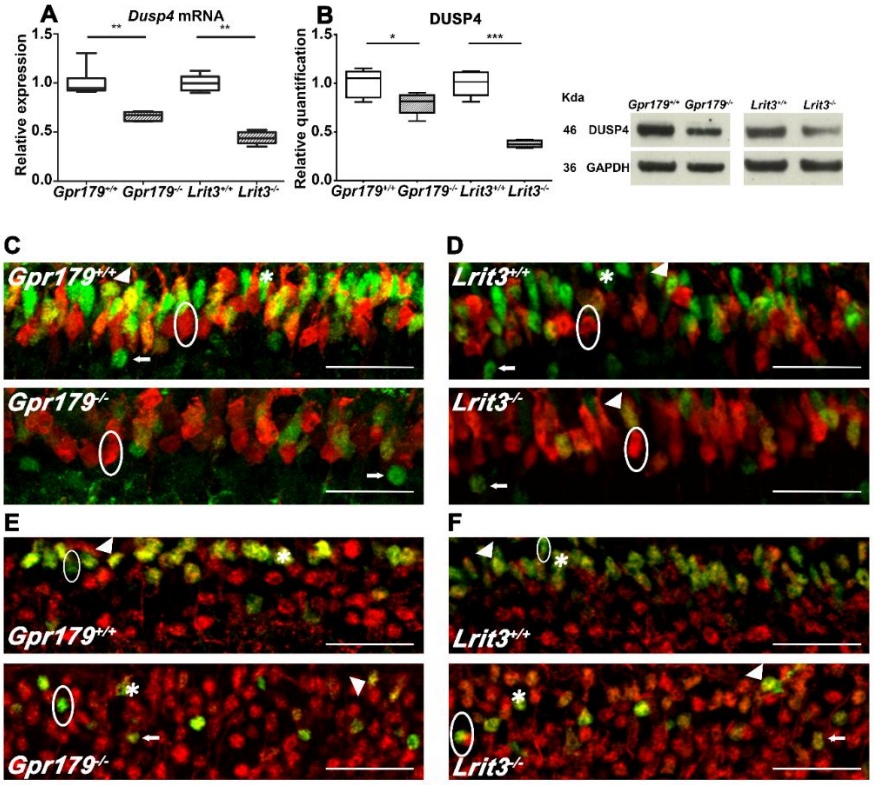

Figure 3: Impact of ON-pathway activity upon DUSP4 expression.

A: Quantification of *Dusp4* mRNA by RT-qPCR performed on isolated adult retinas from two cCSNB mouse models (*Gpr179*$^{-/-}$ and *Lrit3*$^{-/}$, n=6 each^{-}) and their corresponding wild-type littermates (n=6 each). B: Quantification of DUSP4 protein by western blotting performed on isolated adult retinas from two cCSNB mouse models (*Gpr179*$^{-/-}$ and *Lrit3*$^{-/-}$, n=5 each) and their corresponding wild-type littermates (n=5 each). C and D: Co-immunostaining of DUSP4 (green) with SCGN (red) performed on adult retinal slices from either *Gpr179*$^{-/-}$ (C, lower image) or *Lrit3*$^{-/-}$ (D, lower image) and their corresponding wild-type littermates (upper images). E and F: Co-immunostaining of DUSP4 (green) with ISLET1 (red) performed on adult retinal slices from either *Gpr179*$^{-/-}$ (E, lower image) or *Lrit3*$^{-/-}$ (F, lower image) and their corresponding littermates (upper images). Scale bars= 50µm. Arrowheads= cone ON-BCs (DUSP4 positive, SCGN or ISLET1 positive, upper part of the INL), stars= RBCs (DUSP4 positive or negative, SCGN negative, ISLET1 positive, upper part of the INL), arrows= potential ACs (DUSP4 positive, SCGN negative, ISLET1 positive, lower part of the INL),

circles= potential OFF-BCs (SCGN positive, ISLET1 negative, DUSP4 positive or negative, lower part of the INL). *: P≤ 0.05, **: p-value≤ 0.01 ***: P≤ 0.001

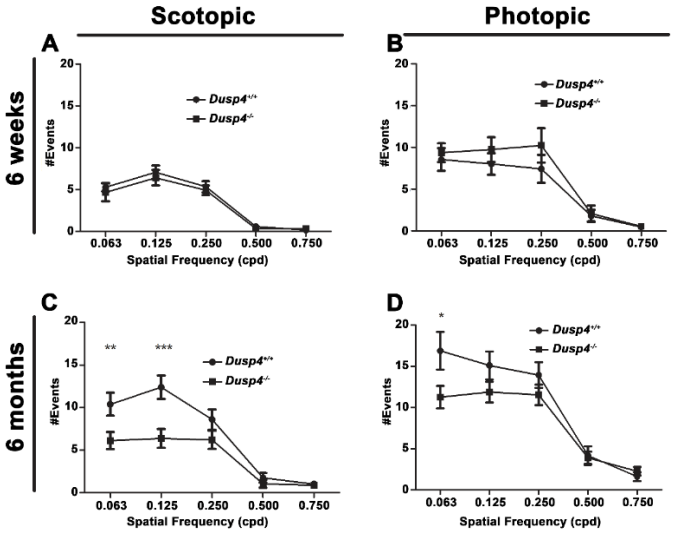

Figure 4: Altered optomotor response in *Dusp4*$^{-/-}$ mice.

A and B: Number of positive events obtained with 6-week-old *Dusp4*$^{-/-}$ mice and their wild-type littermates under scotopic (A, n=9-11) and photopic (B, n=8 each) conditions. C and D: Number of positive events obtained with 6-month-old *Dusp4*$^{-/-}$ mice and their wild-type littermates under scotopic (C, n=10-12) and photopic (D, n=10-12) conditions. Cpd= cycles per degree. ns= non-significant, *: P≤ 0.05, **:P≤ 0.01 ***: P≤ 0.001.

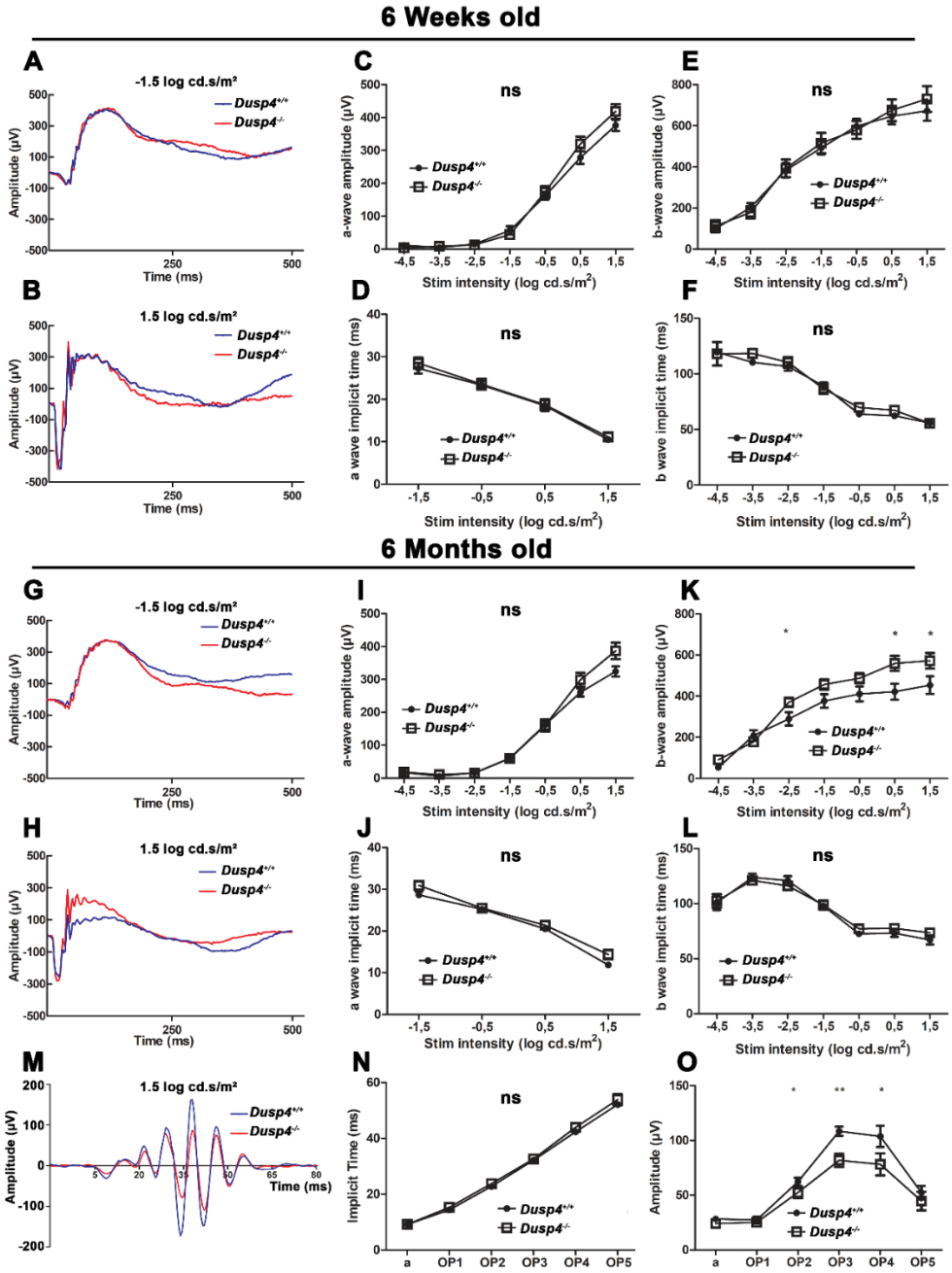

Figure 5: Altered b-wave and OPs observed in *Dusp4*$^{-/-}$ mice.

A to F: Measurement of the amplitude (C and E) and implicit time (D and F) of the ERG a-wave and b-wave in response to flashes of increasing intensities recorded from 6-week-old *Dusp4*$^{-/-}$ (n=9) and their wild-type littermates (n=8). A and B show representatives ERG traces at -1.5 log cd.s/m² and 1.5 log cd.s/m², respectively. G to L: Measurement of the amplitude (I and K) and implicit time

(J and L) of a-wave and b-wave in response to flashes of increasing intensities recorded from 6-month-old *Dusp4*$^{-/-}$ (n=10) and their wild-type littermates (n=9). G and H show representatives ERG traces at -1.5 log cd.s/m² and 1.5 log cd.s/m², respectively.

M to O: Measurement of implicit time (N) and amplitudes (O) of the a-wave (x axis: a) and the OPs (x axis: OP1 to OP5) elicited by flashes of 1.5 log cd.s/m² from 6-month-old *Dusp4*$^{-/-}$ mice (n=11) and their wild-type littermates (n=13). M shows a representative trace of the filtered OPs signal. ns= non-significant, *: P≤ 0.05, **:P≤ 0.01.

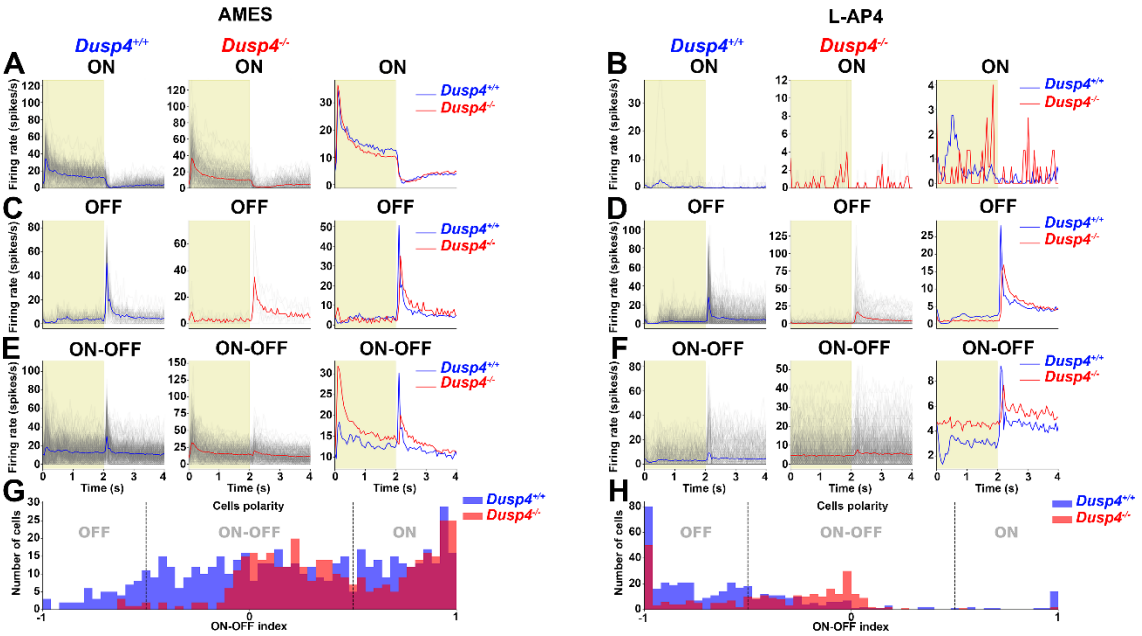

I

AMES	ON		OFF		ON-OFF		Total	
	N	% total	N	% total	N	% total	N	% total
Dusp4$^{+/+}$	183	34,79	53	10,07	290	55,13	526	100
Dusp4$^{-/-}$	151	41,82	6	1,66	204	56,51	361	100

J

L-AP4	ON		OFF		ON-OFF		Total	
	N	% total	N	% total	N	% total	N	% total
Dusp4$^{+/+}$	21	3,99	268	50,95	237	45,05	526	100
Dusp4$^{-/-}$	3	0,83	106	29,36	252	69,81	361	100

Figure 6: Altered ON and OFF RGCs signaling in *Dusp4*$^{-/-}$ mice. Mean spiking rate of ON-RGCs (A: 183 *Dusp4*$^{+/+}$ cells, 151 *Dusp4*$^{-/-}$ cells and B: 21 *Dusp4*$^{+/+}$ cells, 3 *Dusp4*$^{-/-}$ cells), OFF RGCs (C: 53 *Dusp4*$^{+/+}$ cells, 6 *Dusp4*$^{-/-}$ cells and D: 268 *Dusp4*$^{+/+}$ cells, 106 *Dusp4*$^{-/-}$ cells), ON-OFF RGCs (E: 290 *Dusp4*$^{+/+}$ cells, 204 *Dusp4*$^{-/-}$ cells and F: 237 *Dusp4*$^{+/+}$ cells, 252 *Dusp4*$^{-/-}$ cells), distribution of RGCs (G and H) according to their response to light onset (ON) or offset (OFF) or both (ON-OFF) and summary of the number and proportion of recorded cells for each condition (I and J) in isolated *Dusp4*$^{+/+}$ (blue, n=2) and *Dusp4*$^{-/-}$ (red, n=2) retinas under normal AMES (left) or L-AP4 (right) perfusion. Yellow parts represent the light stimulus.

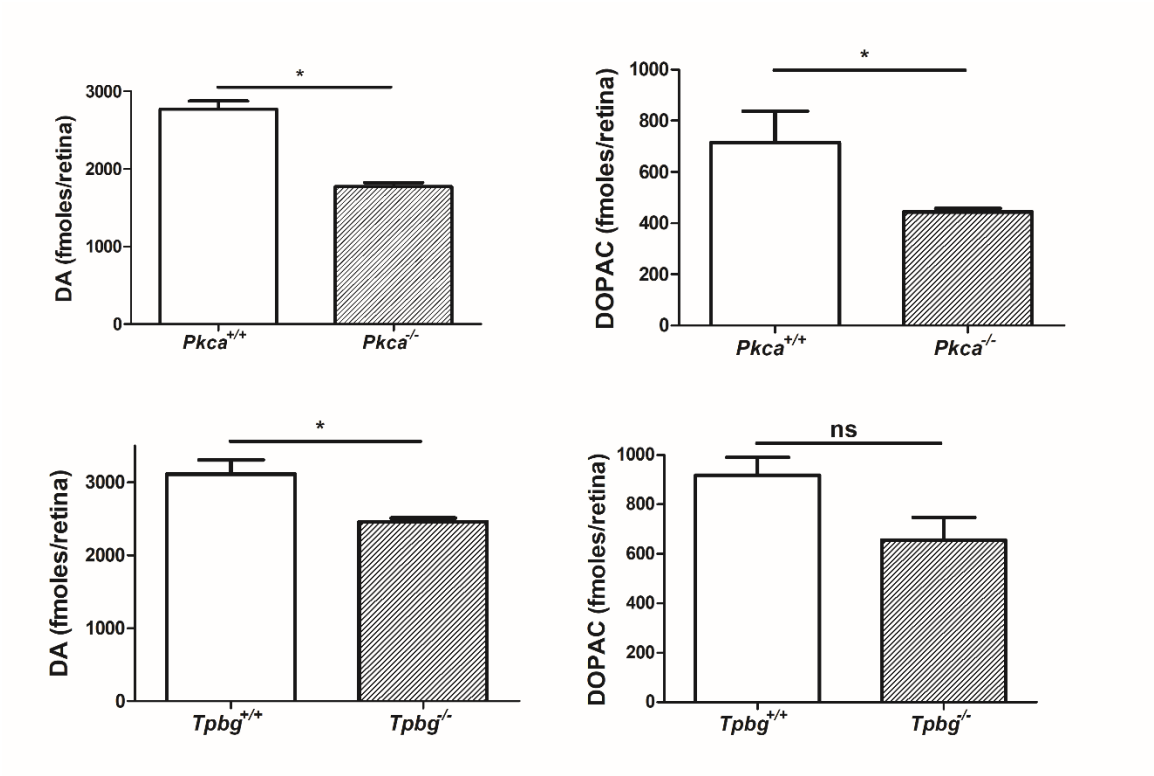

Supplemental figure 1: Reduced levels of DA and DOPAC in *Pkcα*$^{-/-}$ and *Tpbg*$^{-/-}$ retinas.

Measurement of retinal levels of DA (left panels) and DOPAC (right panels) in adult light-adapted *Pkcα*$^{-/-}$, *Pkcα*$^{+/+}$ (upper panels) and *Tpbg*$^{-/-}$, *Tpbg*$^{+/+}$ (lower panels) mice using UPLC (n=3 each). ns= non-significant, *: p-value ≤0.05.

Supplemental figure 2: No change of retinal layers thickness in *Dusp4*$^{-/-}$ mice.

Inner plexiform layer and inner nuclear layer assessed using SD-OCT from 6-week-old and 6-month-old *Dusp4*$^{+/+}$ and *Dusp4*$^{-/-}$ mice. The layer thickness is represented according to the distance from the optic disc on both temporo-nasal (T⇔N) and ventro-dorsal (V⇔D) axis. ns= non-significant.

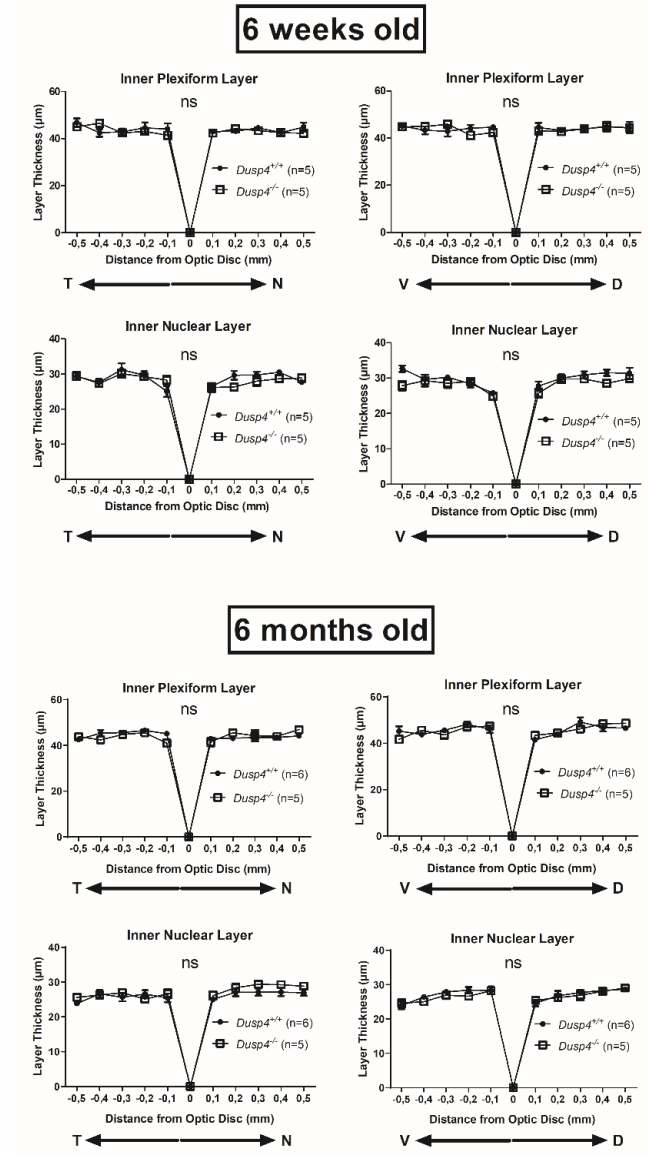

References

1. Wu, P.C., et al., *Epidemiology of Myopia.* Asia Pac J Ophthalmol (Phila), 2016. **5**(6): p. 386-393.
2. Dolgin, E., *The myopia boom.* Nature News, 2015. **519**(7543): p. 276.
3. Morgan, I.G., K. Ohno-Matsui, and S.M. Saw, *Myopia.* Lancet, 2012. **379**(9827): p. 1739-48.
4. Ikuno, Y., *OVERVIEW OF THE COMPLICATIONS OF HIGH MYOPIA.* Retina, 2017. **37**(12): p. 2347-2351.
5. Zeitz, C., A.G. Robson, and I. Audo, *Congenital stationary night blindness: An analysis and update of genotype–phenotype correlations and pathogenic mechanisms.* Progress in Retinal and Eye Research, 2015. **45**: p. 58-110.
6. Igelman, A.D., et al., *Characterising the refractive error in paediatric patients with congenital stationary night blindness: a multicentre study.* Br J Ophthalmol, 2024.
7. Poels, M.M.F., et al., *Natural Course of Refractive Error in Congenital Stationary Night Blindness: Implications for Myopia Treatment.* Invest Ophthalmol Vis Sci, 2024. **65**(14): p. 9.
8. Zhou, X., et al., *Dopamine signaling and myopia development: What are the key challenges.* Progress in Retinal and Eye Research, 2017. **61**: p. 60-71.
9. Feldkaemper, M. and F. Schaeffel, *An updated view on the role of dopamine in myopia.* Experimental Eye Research, 2013. **114**: p. 106-119.
10. Huang, F., et al., *Retinal Dopamine D2 Receptors Participate in the Development of Myopia in Mice.* Invest Ophthalmol Vis Sci, 2022. **63**(1): p. 24.
11. Yin, X. and J. Ge, *The Role of Scleral Changes in the Progression of Myopia: A Review and Future Directions.* Clin Ophthalmol, 2025. **19**: p. 1699-1707.
12. Landis, E.G., et al., *Ambient Light Regulates Retinal Dopamine Signaling and Myopia Susceptibility.* Invest Ophthalmol Vis Sci, 2021. **62**(1): p. 28.
13. Thomson, K., C. Karouta, and R. Ashby, *Form-Deprivation and Lens-Induced Myopia Are Similarly Affected by Pharmacological Manipulation of the Dopaminergic System in Chicks.* Invest Ophthalmol Vis Sci, 2020. **61**(12): p. 4.
14. Pardue, M.T., et al., *High susceptibility to experimental myopia in a mouse model with a retinal ON pathway defect.* Investigative ophthalmology & visual science, 2008. **49**(2): p. 706-712.
15. Chakraborty, R., et al., *ON pathway mutations increase susceptibility to form-deprivation myopia.* Exp Eye Res, 2015. **137**: p. 79-83.
16. Wilmet, B., et al., *Mice Lacking Gpr179 with Complete Congenital Stationary Night Blindness Are a Good Model for Myopia.* Int J Mol Sci, 2022. **24**(1).
17. Zeitz, C., et al., *Shedding light on myopia by studying complete congenital stationary night blindness.* Prog Retin Eye Res, 2023. **93**: p. 101155.
18. Wilmet, B., et al., *Loss of ON-Pathway Function in Mice Lacking Lrit3 Decreases Recovery From Lens-Induced Myopia.* Invest Ophthalmol Vis Sci, 2024. **65**(11): p. 18.
19. Al-Mutairi, M.S., et al., *MAP Kinase Phosphatase-2 Plays a Critical Role in Response to Infection by Leishmania mexicana.* PLoS Pathogens, 2010. **6**(11).
20. Chen, M., et al., *Compound haploinsufficiency of Dok2 and Dusp4 promotes lung tumorigenesis.* J Clin Invest, 2019. **129**(1): p. 215-222.

21. Barajas-Espinosa, A., et al., *Modulation of p38 kinase by DUSP4 is important in regulating cardiovascular function under oxidative stress.* Free Radic Biol Med, 2015. **89**: p. 170-81.
22. Kirchner, A., et al., *DUSP4 appears to be a highly localized endogenous inhibitor of epileptic signaling in human neocortex.* Neurobiology of Disease, 2020. **145**: p. 105073.
23. Balko, J.M., et al., *Activation of MAPK pathways due to DUSP4 loss promotes cancer stem cell-like phenotypes in basal-like breast cancer.* Cancer Res, 2013. **73**(20): p. 6346-58.
24. Barajas-Espinosa, A., et al., *Redox activation of DUSP4 by N-acetylcysteine protects endothelial cells from Cd^{2+}-induced apoptosis.* Free Radic Biol Med, 2014. **74**: p. 188-199.
25. Teng, C.H., W.N. Huang, and T.C. Meng, *Several dual specificity phosphatases coordinate to control the magnitude and duration of JNK activation in signaling response to oxidative stress.* J Biol Chem, 2007. **282**(39): p. 28395-28407.
26. Liu, X., et al., *The Protective Role of DUSP4 in Retinal Pigment Epithelium Senescence and Degeneration.* Int J Mol Sci, 2025. **26**(8).
27. She, M., et al., *Modulation of the ERK1/2-MMP-2 pathway in the sclera of guinea pigs following induction of myopia by flickering light.* Exp Ther Med, 2021. **21**(4): p. 371.
28. McGlinn, A.M., et al., *Form-deprivation myopia in chick induces limited changes in retinal gene expression.* Invest Ophthalmol Vis Sci, 2007. **48**(8): p. 3430-6.
29. Tkatchenko, A.V., et al., *Large-Scale microRNA Expression Profiling Identifies Putative Retinal miRNA-mRNA Signaling Pathways Underlying Form-Deprivation Myopia in Mice.* PLoS One, 2016. **11**(9): p. e0162541.
30. Klopocki, E., et al., *A novel 8 Mb interstitial deletion of chromosome 8p12-p21.2.* Am J Med Genet A, 2006. **140**(8): p. 873-7.
31. Bergen, M.A., et al., *Altered Refractive Development in Mice With Reduced Levels of Retinal Dopamine.* Invest Ophthalmol Vis Sci, 2016. **57**(10): p. 4412-4419.
32. Qian, K.W., et al., *Altered Retinal Dopamine Levels in a Melatonin-proficient Mouse Model of Form-deprivation Myopia.* Neurosci Bull, 2022. **38**(9): p. 992-1006.
33. Pardue, M.T., et al., *High susceptibility to experimental myopia in a mouse model with a retinal on pathway defect.* Invest Ophthalmol Vis Sci, 2008. **49**(2): p. 706-12.
34. Peachey, N.S., et al., *Depolarizing bipolar cell dysfunction due to a Trpm1 point mutation.* Journal of Neurophysiology, 2012. **108**(9): p. 2442-2451.
35. Peachey, Neal S., et al., *GPR179 Is Required for Depolarizing Bipolar Cell Function and Is Mutated in Autosomal-Recessive Complete Congenital Stationary Night Blindness.* The American Journal of Human Genetics, 2012. **90**(2): p. 331-339.
36. Park, J.C., et al., *Effects of normal aging on the mouse retina assessed by full-field flash and flicker electroretinography.* Sci Rep, 2023. **13**(1): p. 8860.
37. Thomas, G.M. and R.L. Huganir, *MAPK cascade signalling and synaptic plasticity.* Nat Rev Neurosci, 2004. **5**(3): p. 173-83.
38. Xiong, W.H., et al., *The Effect of PKCα on the Light Response of Rod Bipolar Cells in the Mouse Retina.* Invest Ophthalmol Vis Sci, 2015. **56**(8): p. 4961-74.
39. Wakeham, C.M., et al., *Trophoblast glycoprotein is required for efficient synaptic vesicle exocytosis from retinal rod bipolar cells.* Front Cell Neurosci, 2023. **17**: p. 1306006.
40. Duvoisin, R., et al., *Increased susceptibility to myopia in Prkca-/- mice, which lack PKCα, a marker of rod bipolar cells.* Investigative Ophthalmology & Visual Science, 2024. **65**(7): p. 3927-3927.

41. Kushner, S.A., et al., *Modulation of presynaptic plasticity and learning by the H-ras/extracellular signal-regulated kinase/synapsin I signaling pathway.* J Neurosci, 2005. **25**(42): p. 9721-34.
42. Giachello, C.N., et al., *MAPK/Erk-dependent phosphorylation of synapsin mediates formation of functional synapses and short-term homosynaptic plasticity.* J Cell Sci, 2010. **123**(Pt 6): p. 881-93.
43. Abdul Rahman, N.Z., et al., *Mitogen-Activated Protein Kinase Phosphatase-2 Deletion Impairs Synaptic Plasticity and Hippocampal-Dependent Memory.* The Journal of Neuroscience, 2016. **36**(8): p. 2348-2354.
44. Tyssowski, K.M., et al., *Different Neuronal Activity Patterns Induce Different Gene Expression Programs.* Neuron, 2018. **98**(3): p. 530-546.e11.
45. Corradi, L., et al., *Hypothalamic Galanin-producing neurons regulate stress in zebrafish through a peptidergic, self-inhibitory loop.* Curr Biol, 2022. **32**(7): p. 1497-1510.e5.
46. Corradi, L., et al., *Using pERK immunostaining to quantify neuronal activity induced by stress in zebrafish larvae.* STAR Protoc, 2022. **3**(4): p. 101731.
47. Pérez-Sen, R., et al., *Dual-Specificity Phosphatase Regulation in Neurons and Glial Cells.* Int J Mol Sci, 2019. **20**(8).
48. Stone, R.A., et al., *Diurnal retinal and choroidal gene expression patterns support a role for circadian biology in myopia pathogenesis.* Sci Rep, 2024. **14**(1): p. 533.
49. Shekhar, K., et al., *Comprehensive Classification of Retinal Bipolar Neurons by Single-Cell Transcriptomics.* Cell, 2016. **166**(5): p. 1308-1323.e30.
50. Fan, W.J., et al., *Neural differentiation and synaptogenesis in retinal development.* Neural Regen Res, 2016. **11**(2): p. 312-8.
51. Hellmer, C.B., et al., *Cholinergic feedback to bipolar cells contributes to motion detection in the mouse retina.* Cell Rep, 2021. **37**(11): p. 110106.
52. Petit-Jacques, J., et al., *Spontaneous oscillatory activity of starburst amacrine cells in the mouse retina.* J Neurophysiol, 2005. **94**(3): p. 1770-80.
53. Petit-Jacques, J. and S.A. Bloomfield, *Synaptic regulation of the light-dependent oscillatory currents in starburst amacrine cells of the mouse retina.* J Neurophysiol, 2008. **100**(2): p. 993-1006.
54. Yoshida, K., et al., *A key role of starburst amacrine cells in originating retinal directional selectivity and optokinetic eye movement.* Neuron, 2001. **30**(3): p. 771-80.
55. Demb, J.B., *Cellular mechanisms for direction selectivity in the retina.* Neuron, 2007. **55**(2): p. 179-86.
56. Weng, S., W. Sun, and S. He, *Identification of ON-OFF direction-selective ganglion cells in the mouse retina.* J Physiol, 2005. **562**(Pt 3): p. 915-23.
57. Fain, G. and A.P. Sampath, *Rod and cone interactions in the retina.* F1000Res, 2018. **7**.
58. Zaghloul, K.A., K. Boahen, and J.B. Demb, *Different circuits for ON and OFF retinal ganglion cells cause different contrast sensitivities.* J Neurosci, 2003. **23**(7): p. 2645-54.
59. Strettoi, E., et al., *Complexity of retinal cone bipolar cells.* Prog Retin Eye Res, 2010. **29**(4): p. 272-83.
60. Chakraborty, R., et al., *Comparison of refractive development and retinal dopamine in OFF pathway mutant and C57BL/6J wild-type mice.* Mol Vis, 2014. **20**: p. 1318-27.
61. Hoseini-Yazdi, H., et al., *Retinal OFF-Pathway Overstimulation Leads to Greater Accommodation-Induced Choroidal Thinning.* Invest Ophthalmol Vis Sci, 2021. **62**(13): p. 5.

62. Jiang, X., et al., *Electrical responses from human retinal cone pathways associate with a common genetic polymorphism implicated in myopia.* Proc Natl Acad Sci U S A, 2022. **119**(21): p. e2119675119.
63. Tkatchenko, A.V., et al., *APLP2 Regulates Refractive Error and Myopia Development in Mice and Humans.* PLoS Genet, 2015. **11**(8): p. e1005432.
64. Dinet, V., et al., *Amyloid Precursor-Like Protein 2 deletion-induced retinal synaptopathy related to congenital stationary night blindness: structural, functional and molecular characteristics.* Mol Brain, 2016. **9**(1): p. 64.
65. Jiang, X., et al., *A highly efficient murine model of experimental myopia.* Scientific Reports, 2018. **8**(1): p. 2026.
66. Schaeffel, F., et al., *Measurement of refractive state and deprivation myopia in two strains of mice.* Optometry and Vision Science: Official Publication of the American Academy of Optometry, 2004. **81**(2): p. 99-110.
67. Orhan, E., et al., *Further insights into GPR179: expression, localization, and associated pathogenic mechanisms leading to complete congenital stationary night blindness.* Invest Ophthalmol Vis Sci, 2013. **54**(13): p. 8041-50.
68. Abdeljalil, J., et al., *The optomotor response: a robust first-line visual screening method for mice.* Vision Res, 2005. **45**(11): p. 1439-46.
69. Varin, J., et al., *Substantial restoration of night vision in adult mice with congenital stationary night blindness.* Mol Ther Methods Clin Dev, 2021. **22**: p. 15-25.
70. Yger, P., et al., *A spike sorting toolbox for up to thousands of electrodes validated with ground truth recordings in vitro and in vivo.* Elife, 2018. **7**.